

Thermal conductivity and thermal boundary resistance of atomic layer deposited high-k dielectric aluminum oxide, hafnium oxide, and titanium oxide thin films on silicon

Ethan A. Scott, John T. Gaskins, Sean W. King, and Patrick E. Hopkins

Citation: [APL Materials](#) **6**, 058302 (2018); doi: 10.1063/1.5021044

View online: <https://doi.org/10.1063/1.5021044>

View Table of Contents: <http://aip.scitation.org/toc/apm/6/5>

Published by the [American Institute of Physics](#)

Articles you may be interested in

[Structural analysis of LaVO₃ thin films under epitaxial strain](#)

APL Materials **6**, 046102 (2018); 10.1063/1.5021844

[Defect phase diagram for doping of Ga₂O₃](#)

APL Materials **6**, 046103 (2018); 10.1063/1.5019938

[Synthesis and electronic properties of Fe₂TiO₅ epitaxial thin films](#)

APL Materials **6**, 056101 (2018); 10.1063/1.5025569

[Lifetime laser damage performance of \$\beta\$ -Ga₂O₃ for high power applications](#)

APL Materials **6**, 036105 (2018); 10.1063/1.5021603

[Highly conductive PdCoO₂ ultrathin films for transparent electrodes](#)

APL Materials **6**, 046107 (2018); 10.1063/1.5027579

[Homogeneous molybdenum disulfide tunnel diode formed via chemical doping](#)

Applied Physics Letters **112**, 183103 (2018); 10.1063/1.5023695

PHYSICS TODAY

WHITEPAPERS

ADVANCED LIGHT CURE ADHESIVES

Take a closer look at what these environmentally friendly adhesive systems can do

READ NOW

PRESENTED BY
 MASTERBOND
ADHESIVES | SEALANTS | COATINGS

Thermal conductivity and thermal boundary resistance of atomic layer deposited high-*k* dielectric aluminum oxide, hafnium oxide, and titanium oxide thin films on silicon

Ethan A. Scott,¹ John T. Gaskins,¹ Sean W. King,²
and Patrick E. Hopkins^{1,3,4,a}

¹*Department of Mechanical and Aerospace Engineering, University of Virginia, Charlottesville, Virginia 22904, USA*

²*Logic Technology Development, Intel Corporation, Hillsboro, Oregon 97124, USA*

³*Department of Materials Science and Engineering, University of Virginia, Charlottesville, Virginia 22904, USA*

⁴*Department of Physics, University of Virginia, Charlottesville, Virginia 22904, USA*

(Received 30 December 2017; accepted 29 April 2018; published online 14 May 2018)

The need for increased control of layer thickness and uniformity as device dimensions shrink has spurred increased use of atomic layer deposition (ALD) for thin film growth. The ability to deposit high dielectric constant (high-*k*) films via ALD has allowed for their widespread use in a swath of optical, optoelectronic, and electronic devices, including integration into CMOS compatible platforms. As the thickness of these dielectric layers is reduced, the interfacial thermal resistance can dictate the overall thermal resistance of the material stack compared to the resistance due to the finite dielectric layer thickness. Time domain thermoreflectance is used to interrogate both the thermal conductivity and the thermal boundary resistance of aluminum oxide, hafnium oxide, and titanium oxide films on silicon. We calculate a representative design map of effective thermal resistances, including those of the dielectric layers and boundary resistances, as a function of dielectric layer thickness, which will be of great importance in predicting the thermal resistances of current and future devices. © 2018 Author(s). All article content, except where otherwise noted, is licensed under a Creative Commons Attribution (CC BY) license (<http://creativecommons.org/licenses/by/4.0/>). <https://doi.org/10.1063/1.5021044>

The thermal conductivity and thermal boundary resistance between device layers play a role in the overall thermal resistance of devices, especially as device layers in a variety of applications are routinely on the order of sub-100 nm.^{1,2} These thermal resistances are of critical importance in consideration of current and future CMOS device performance and reliability. For example, there has been recent interest in advancing and improving fin field effect transistors (FinFETs), as their geometry yields electronic properties which identify them as highly favorable candidates for future CMOS devices; however, there are challenges associated with self-heating and heat dissipation.³ The low thermal conductivity of the high dielectric constant materials (high-*k* dielectric materials) within the devices leads to self-induced thermal runaway and breakdown. Simulations have been performed to model and gain further insight into the problem;^{4,5} however, the thermal boundary resistances (TBRs)^{6,7} at the high-*k* dielectric materials' interfaces are often neglected.

Furthermore, while the overwhelming majority of studies have focused on the electronic properties of ALD high-*k* dielectrics, few studies have reported on thermal conductivity measurements on ALD Al₂O₃,^{8–11} HfO₂,^{8,9,12} and TiO₂ films.^{13,14} This gap in the literature is due in large part to difficulties in measuring the thermal conductivity of thin films with thicknesses of interest for

^aAuthor to whom correspondence should be addressed: phopkins@virginia.edu

high- k dielectric layers in CMOS devices (<10–20 nm). At these length scales, the TBR at the high- k dielectric interfaces can dominate the overall resistance, and thus, the thermal conductivity of the high- k dielectric film can be difficult to isolate. Furthermore, the variability of TBR with extrinsic parameters such as surface roughness,^{7,15–17} interfacial bonding environment,^{18–26} and other defects at or near the interface^{27–33} makes the measurement of the thermal conductivity, κ , of ALD-grown thin films and their respective TBRs most critical on samples fabricated under conditions consistent with current and future CMOS devices.

In this letter, we report the thermal conductivity, TBR, and total thermal resistance for ALD-grown Al₂O₃, HfO₂, and TiO₂ thin films on silicon substrates via time domain thermoreflectance (TDTR). These films are grown using industry standard conditions presently of interest to current and future CMOS technologies. We prepare samples with thicknesses ranging from 1 to 10 nm and apply a series resistor model for the total thermal resistance of the sample, from which we calculate the intrinsic thermal conductivity of the films and the TBR at the films' interfaces. A representative design map of effective thermal resistances, including those of the dielectric layers and boundary resistances, as a function of dielectric layer thickness, is presented for the samples tested. This design map will be of great importance in predicting the thermal resistances of current and future devices.

Deposition conditions and details of the high- k dielectric fabrication have been previously reported.^{34–36} All films were grown on double-side polished (001) silicon substrates at temperatures on the order of 300 °C using industry standard precursors and commercially available ALD tools.^{34,37} The silicon substrates were not subjected to an HF preclean and, as such, the native oxide remained on the wafers prior to ALD. Al₂O₃ and HfO₂ films were fabricated with nominal thicknesses of 1, 3, 5, and 10 nm. Films of 1, 3, and 10 nm were additionally fabricated for TiO₂. Thicknesses were verified with X-ray reflectivity (XRR), which were all within 7% of the nominal value. For some of the thinnest films, the thickness was not measurable, and a thickness uncertainty of 5% was assumed.

Thermal properties were measured using TDTR³⁸ in a “two-tint” configuration.³⁹ TDTR is an optical pump probe measurement utilizing a short-pulsed laser system to both induce and monitor an oscillatory heating event on the surface of a metallic film opto-thermal transducer as a function of pump-probe delay time. The output of an 80 MHz Ti:sapphire oscillator (Spectra-Physics Tsunami) centered at 808 nm was spectrally split into a pump path, which was modulated using an electro-optical modulator (EOM) at 8.4 MHz, and a time delayed probe path. The pump and probe beams were collinearly focused on the surface of an ~80 nm aluminum film that was electron-beam evaporated on top of the dielectric samples, serving as the aforementioned opto-thermal transducer. A beam profiler was used to measure the $1/e^2$ diameter of the pump and probe, which were 32 and 12 μm , respectively. The reflectivity of the probe beam at the pump modulation frequency was monitored via a photodiode, and the in-phase and out-of-phase signals relative to the pump modulation frequency trigger are extracted using a RF lock-in amplifier. Further details on the TDTR measurement and model used to extract thermophysical properties are detailed extensively elsewhere.^{7,38,40,41}

Characterization of density and thickness were performed via nuclear reaction analysis-Rutherford backscattering (NRA-RBS)⁴² and XRR,⁴³ respectively. HfO₂ and TiO₂ were found to have densities comparable to the bulk, whereas the Al₂O₃ samples had densities averaging 3.3 g cm⁻³ which is 15% less than the theoretical bulk density of 3.9 g cm⁻³.⁴⁴ Variations from the bulk density were used to proportionally scale the assumption for heat capacity of films used in thermal calculations. Furthermore, picosecond acoustics^{45,46} and mechanical profilometry were used to measure the film thickness of the aluminum transducer. The relevant sample details are presented in Table I.

As the thickness of the Al₂O₃, HfO₂, and TiO₂ films ranged from 1 to 10 nm, there was insufficient sensitivity to measure the individual thermal resistances with TDTR. Instead, the film resistance and its associated interfacial resistances were treated as a singular, effective interface between the aluminum transducer and silicon substrate. Dividing the film thickness by this effective resistance provides an effective thermal conductivity, as shown in Fig. 1. The error bars represent the uncertainty associated with the repeatability of sample measurement with TDTR in addition to the standard

TABLE I. Summary of thermal properties for the ALD high- k dielectrics investigated in this study along with relevant sample details. κ is the intrinsic thermal conductivity of the high- k dielectric film and TBR is the total interfacial resistance across both interfaces of the film. Note: *NM* = not measurable (too thin). For these films, we assume the nominal thickness value with 5% uncertainty.

Film	κ (W m ⁻¹ K ⁻¹)	TBR (m ² K GW ⁻¹)	Density (g cm ⁻³)	Nominal thickness (nm)	Thickness (XRR) (nm)
Al ₂ O ₃	1.50 ± 0.09	6.92 ± 0.50	3.33 ± 0.06	1	<i>NM</i>
				3	<i>NM</i>
				5	4.67
				10	9.39
HfO ₂	1.00 ± 0.06	9.03 ± 0.66	10.33 ± 0.36	1	<i>NM</i>
				3	3.11
				5	5.07
				10	9.74
TiO ₂	2.52 ± 0.07	8.01 ± 0.71	4.1 ± 0.14	1	<i>NM</i>
				3	<i>NM</i>
				10	10.11

deviation in the measurement of the thickness of the aluminum transducer and thickness of the ALD film. By applying a series resistor model that treats the total resistance as a summation of the film and interfacial resistances,⁴⁷ the intrinsic film thermal conductivity and total interfacial resistance are then deconvolved from the effective thermal conductivity with the following expression:

$$\kappa_{eff} = \frac{\kappa_i}{1 + \frac{\kappa_i R_{tot}}{d}}, \quad (1)$$

where κ_i is the intrinsic thermal conductivity of the film, R_{tot} is the total interfacial resistance (i.e., the total TBR across both the Al/film and film/Si interfaces), and d is the film thickness. A non-linear least squares model fit was applied to the experimental data with κ_i and R_{tot} as the fitting parameters for each film. The intrinsic thermal conductivities and thermal boundary resistances for the films determined via Eq. (1) are listed in Table I. The corresponding uncertainties are obtained by fitting for these parameters at the experimental upper and lower bounds for κ_{Eff} .

We find good agreement between the model and experimentally measured values for effective thermal conductivity. The resultant intrinsic thermal conductivities of the Al₂O₃ films are within the range of previous measurements of amorphous ALD-grown Al₂O₃.^{8–11} While several reports on the thermal conductivity of HfO₂ thin films exist in the literature (for a review, see Ref. 8), they range in deposition technique and crystallinity. We are only aware of one previous work on the thermal

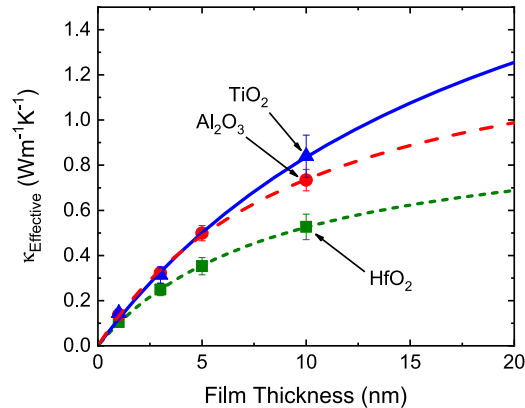


FIG. 1. Measured effective thermal conductivities of TiO₂ (triangles), Al₂O₃ (circles), and HfO₂ (squares) films ranging from 1 to 10 nm. A series thermal resistor model [Eq. (1)] is applied to the data for which the intrinsic thermal conductivity and total thermal boundary resistance are the fitting parameters. The best fits are shown as the lines in the plot.

conductivity of a purely amorphous HfO₂ thin film,¹² and they report an intrinsic thermal conductivity of 0.58 W m⁻¹ K⁻¹ (note, we find $\kappa_{i,\text{HfO}_2} = 1.00 \text{ W m}^{-1} \text{ K}^{-1}$, cf. Table I). We are currently unaware of the reason for the difference in these reported values. However, we note that Ref. 12 does not report the density of their HfO₂ films, and any difference in density could result in changes in thermal conductivity in the amorphous films, as we have previously shown in ALD-grown Al₂O₃.¹⁰ Given the differences in growth temperatures of the ALD films grown in this work compared to those grown in Ref. 12 (along with other possible differences in fabrication procedures), a difference in density being at least the partial source of the discrepancies in reported κ_{i,HfO_2} is a reasonable speculation. The measured thermal conductivity of our ALD-grown TiO₂ films is nearly a factor of 2 higher than that reported for an amorphous ALD-grown TiO₂ film from our previous work.¹³ Our current films are more dense than those we previously measured in Ref. 13 (densities listed in Table II), which can account for part of this difference.¹⁰ However, another possible explanation could be due to the partial crystallization of our current ALD TiO₂ films with increasing thickness. Mitchell *et al.*⁴⁸ demonstrated that for ALD-grown TiO₂ films deposited under nearly identical conditions (Si substrate with native oxide, deposition temperatures between 250 and 300 °C), the films remain amorphous for thicknesses on the order of 2.4 nm and begin to crystallize at thicknesses of 20 nm. As the TiO₂ films in this study included thicknesses of 1, 3, and 10 nm, it is possible that the thicker films in our study are actually partially crystalline, which would increase the thermal conductivity. The effects of the onset of crystallinity on the thermal conductivity of ALD grown TiO₂ are beyond the scope of this current work. A summary of previous reports of the thermal conductivity of ALD-grown amorphous thin films compared to those reported in this current work, along with ranges of thicknesses and densities, is given in Table II.

The thermal conductivity and total TBR, shown in Table I, are recast as a combined effective thermal resistance as a function of dielectric layer thickness in Fig. 2. The black lines in Figs. 2(a)–2(c) represent the total effective thermal resistance. This includes the resistance attributed to the aluminum/film interface, resistance inherent to the film, and also that of the film/substrate interface. To approximate the thermal resistance contribution from the film/substrate interface, we subtract the resistance from the aluminum/film interface. As we are insensitive to measurements of this value, we assume a resistance at the aluminum/high-*k* dielectric film interface of 3.34–6.67 m² K GW⁻¹ which spans a range representative of what is found in the literature for Al/dielectric interfaces.^{7,49} The shaded regions in Figs. 2(a)–2(c) then represent the upper and lower bounds for the thermal resistance attributed to the film and film/silicon substrate interface. In other words, the lower bound of the shaded region represents the lower limit to the thermal resistance which can be attributed to the ALD film plus the film/substrate interface and vice versa for the upper bound of the shaded region.

It is clear that in the limit of a film approaching zero thickness, the TBRs govern the total thermal resistance. We also note that the Al₂O₃ system offers the most efficient method with which to dissipate heat for films of thickness less than 10 nm, owing to the low TBR at its interfaces relative to the other two films. At larger thicknesses, a TiO₂ film on the Si substrate system demonstrates the highest efficiency for heat dissipation as the elevated thermal conductivity compensates for the higher thermal boundary resistance at larger film thicknesses, compared to Al₂O₃. Conversely, HfO₂

TABLE II. Summary of the literature values for thermal conductivity of ALD-grown Al₂O₃, HfO₂, and TiO₂ amorphous thin films. Reported film thicknesses and densities are also included. Also included are the values for the intrinsic thermal conductivities of the films in this study, repeated from Table I.

ALD film	κ (W m ⁻¹ K ⁻¹)	Thickness (nm)	Density (g cm ⁻³)	References
Al ₂ O ₃	1.3–2.6	10–200	2.7–3.1	8–11
Al ₂ O ₃	1.50 ± 0.09	1–10	3.33 ± 0.06	This study
HfO ₂	0.58	5.6	Not reported	12
HfO ₂	1.00 ± 0.06	1–10	10.33 ± 0.36	This study
TiO ₂	1.33	98.3	3.65	13
TiO ₂ ^a	2.55 ± 0.07	1–10	4.1 ± 0.14	This study

^aPossible crystallinity hypothesized in thicker films.

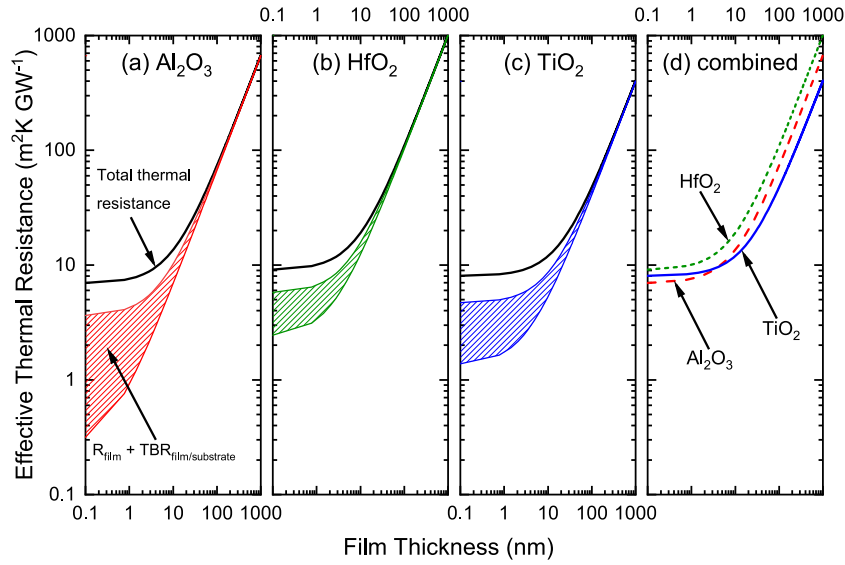


FIG. 2. Effective thermal resistances for ALD-grown high- k dielectric (a) Al_2O_3 , (b) HfO_2 , and (c) TiO_2 films studied in this work. The black lines in each figure display the total thermal resistance. The shaded regions display the combined resistance of the film, R_{film} (where $R_{\text{film}} = d/\kappa_i$, where κ_i is listed in Tables I and II), and film/substrate interface, $\text{TBR}_{\text{film/substrate}}$, assuming an Al/film interfacial resistance between 3.34 and $6.67 \text{ m}^2 \text{ K GW}^{-1}$. (d) combines the effective thermal resistances displayed in (a)–(c) for comparison.

offers the lowest capacity for heat transfer across the measured thickness range due to its high TBR and low thermal conductivity, relative to the Al_2O_3 and TiO_2 on native oxide/silicon substrates.

Clearly, as the sample thicknesses decrease, the overall resistances of the systems become dominated by the dielectric film/Si substrate interface. To gain insight into the mechanisms that lead to the trends in dielectric film/Si substrate TBRs, we contrast our measured TBRs displayed in Fig. 2 to theoretical approximations for TBR from the diffusive mismatch model (DMM)⁶ using a gray approximation.⁵⁰ In this limit, phonon transmissivity from layer i into layer j is calculated as $T_{dij} = \frac{C_j v_j}{C_i v_i + C_j v_j}$, where C and v are the volumetric heat capacity and phonon group velocity, respectively. The TBR is then calculated as $\text{TBR} = \left(\frac{C_i v_i}{4\pi} \frac{C_j v_j}{C_i v_i + C_j v_j} \right)^{-1}$. While more rigorous calculations of the DMM can be performed for these interfaces by, for example, using realistic phonon dispersion relations,^{51,52} our goal in this work is to understand the trends in TBR among the different high- k dielectric film interfaces, and thus, this gray approximation is sufficient. While we caution that the exact TBR that this model predicts will not be an accurate calculation of the actual TBR that we measure, the ratios of TBRs among the different materials should be accurately represented via this approach.

For this first approximation of thermal boundary resistance, we assume literature values of 8800 , 4800 , and 9200 m s^{-1} for the longitudinal sound speed of the Al_2O_3 , HfO_2 , and TiO_2 films, respectively,⁵³ and heat capacities of 2.65 , 2.71 , and $2.83 \text{ J cm}^{-3} \text{ K}^{-1}$ for Al_2O_3 , HfO_2 , and TiO_2 , which were calculated from the molar heat capacities given in Refs. 54, 55, and 54, respectively, and the mass density listed in Table II. Additionally, we assume a volumetric heat capacity and longitudinal sound speed of $1.65 \text{ J cm}^{-3} \text{ K}^{-1}$ and 8433 m s^{-1} , respectively, for the (100) silicon substrate.^{56,57} Using these values in the DMM, we calculate the ratio of film TBRs. A ratio of 1.30 is obtained for $\text{TBR}_{\text{HfO}_2/\text{Si}} \cdot \text{TBR}_{\text{Al}_2\text{O}_3/\text{Si}}$ and 1.35 for $\text{TBR}_{\text{HfO}_2/\text{Si}} \cdot \text{TBR}_{\text{TiO}_2/\text{Si}}$. In other words, the thermal boundary resistance between HfO_2 and silicon is predicted to be at least 1.30 times larger than that of Al_2O_3 and silicon and 1.35 times larger than that of TiO_2 and silicon, as determined via our DMM calculations.

These ratios of TBRs generally capture our experimental observations. For example, in Fig. 2, in the limit of zero film thickness, the TBR of the film/substrate dominates the resistance displayed in the shaded regions. Therefore, in this limit, we approximate the TBR of the film/substrate interface

as the average value of the upper and lower bound of this region. Taking the ratio of these TBRs in the same manner as previously mentioned, we find a TBR ratio of 2.08 for $TBR_{\text{HfO}_2/\text{Si}}:TBR_{\text{Al}_2\text{O}_3/\text{Si}}$ and 1.35 for $TBR_{\text{HfO}_2/\text{Si}}:TBR_{\text{TiO}_2/\text{Si}}$. While the magnitudes of these ratios differ slightly from those found in the diffuse scattering limit model, the trends remain the same. The interfacial resistance of the HfO₂ films is highest, followed by Al₂O₃ and TiO₂. Furthermore, these calculations and their agreement with the relative magnitudes of the measured TBRs suggest that the differences in TBR originate due to the lower vibrational velocities in HfO₂.

In summary, we report on the intrinsic thermal conductivity and thermal boundary resistances of three atomic layer deposited high-*k* dielectric films—Al₂O₃, HfO₂, and TiO₂—with thicknesses ranging from 1 to 10 nm grown on native oxide/Si substrates. Prior reports on the thermal transport properties of amorphous ALD-grown films have remained limited, particularly for HfO₂ and TiO₂. We demonstrate that as the thickness of these dielectric layers is reduced, the effective thermal conductivity reduces proportionally with thickness, and the TBR across the high-*k* dielectric film interfaces becomes the dominant contribution to the overall thermal resistance of the material stack compared to the resistance attributed to the finite dielectric layer thickness and its intrinsic thermal conductivity. We calculate a representative design map of effective thermal resistances, including those of the dielectric layers and boundary resistances, as a function of dielectric layer thickness. We find Al₂O₃ to be the most thermally efficient film for thicknesses in the sub-10 nm regime, which we attribute to the decreased TBR at the Al₂O₃/native oxide/Si interface compared to the other systems. Above this regime, TiO₂ is the most efficient, and for all thicknesses, we find HfO₂ to be the most thermally resistive. This design map will be of great importance in predicting the thermal resistances of current and future devices.

We appreciate support from the Army Research Office (Grant No. W911NF-16-1-0320).

- ¹ T. W. Kim, D. H. Kim, D. H. Koh, H. M. Kwon, R. H. Baek, D. Veksler, C. Huffman, K. Matthews, S. Oktyabrsky, A. Greene, Y. Ohsawa, A. Ko, H. Nakajima, M. Takahashi, T. Nishizuka, H. Ohtake, S. K. Banerjee, S. H. Shin, D. H. Ko, C. Kang, D. Gilmer, R. J. W. Hill, W. Maszara, C. Hobbs, and P. D. Kirsch, "Sub-100 nm InGaAs quantum-well (QW) tri-gate MOSFETs with Al₂O₃/HfO₂ (EOT < 1 nm) for low-power logic applications," in *IEEE International Electron Devices Meeting 2013* (IEEE, 2013).
- ² Y. Song, R. Xu, J. He, S. Siontas, A. Zaslavsky, and D. C. Paine, "Top-gated indium-zinc-oxide thin-film transistors with *in situ* Al₂O₃/HfO₂ gate oxide," *IEEE Electron Device Lett.* **35**, 1251–1253 (2014).
- ³ M. Orouji and M. Mehrdad, "A new rounded edge fin field effect transistor for improving self-heating effects," *Jpn. J. Appl. Phys., Part 2* **50**, 124303 (2011).
- ⁴ L. Wang, A. R. Brown, M. Nedjalkov, C. Alexander, B. Cheng, C. Millar, and A. Asenov, "Impact of self-heating on the statistical variability in bulk and SOI FinFETs," *IEEE Trans. Electron Devices* **62**, 2106–2112 (2015).
- ⁵ M. Zubert, T. Raszkowski, A. Samson, M. Janicki, and A. Napieralski, "The distributed thermal model of fin field effect transistor," *Microelectron. Reliab.* **67**, 9–14 (2016).
- ⁶ E. T. Swartz and R. O. Pohl, "Thermal boundary resistance," *Rev. Mod. Phys.* **61**, 605–668 (1989).
- ⁷ P. E. Hopkins, "Thermal transport across solid interfaces with nanoscale imperfections: Effects of roughness, disorder, dislocations, and bonding on thermal boundary conductance," *ISRN Mech. Eng.* **2013**, 682586.
- ⁸ J. T. Gaskins, P. E. Hopkins, D. R. Merrill, S. R. Bauers, E. Hadland, D. C. Johnson, D. Koh, J. H. Yum, S. Banerjee, B. J. Nordell, M. M. Paquette, A. N. Caruso, W. A. Lanford, P. Henry, L. Ross, H. Li, L. Li, M. French, A. M. Rudolph, and S. W. King, "Review—Investigation and review of the thermal, mechanical, electrical, optical, and structural properties of atomic layer deposited high-*k* dielectrics: Beryllium oxide, aluminum oxide, hafnium oxide, and aluminum nitride," *ACS J. Solid State Sci. Technol.* **6**, N189–N208 (2017).
- ⁹ N. T. Gabriel and J. J. Talghader, "Thermal conductivity and refractive index of hafnia-alumina nanolaminates," *J. Appl. Phys.* **110**, 043526 (2011).
- ¹⁰ C. S. Gorham, J. T. Gaskins, G. N. Parsons, M. D. Losego, and P. E. Hopkins, "Density dependence of the room temperature thermal conductivity of atomic layer deposition grown amorphous alumina (Al₂O₃)," *Appl. Phys. Lett.* **104**, 253107 (2014).
- ¹¹ Z. Luo, H. Liu, B. T. Spann, Y. Feng, P. Ye, Y. P. Chen, and X. Xu, "Measurement of in-plane thermal conductivity of ultrathin films using micro-Raman spectroscopy," *Nanoscale Microscale Thermophys. Eng.* **18**, 183–193 (2014).
- ¹² M. A. Panzer, M. Shandalov, J. A. Rowlette, Y. Oshima, Y. W. Chen, P. C. McIntyre, and K. E. Goodson, "Thermal properties of ultrathin hafnium oxide gate dielectric films," *IEEE Electron Device Lett.* **30**, 1269–1271 (2009).
- ¹³ A. Giri, J.-P. Niemela, C. J. Szwejkowski, M. Karppinen, and P. E. Hopkins, "Reduction in thermal conductivity and tunable heat capacity of inorganic/organic hybrid superlattices," *Phys. Rev. B* **93**, 024201 (2016).
- ¹⁴ J.-P. Niemela, A. Giri, P. E. Hopkins, and M. Karppinen, "Ultra-low thermal conductivity in TiO₂:C superlattices," *J. Mater. Chem. A* **3**, 11527–11532 (2015).
- ¹⁵ P. E. Hopkins, L. M. Phinney, J. R. Serrano, and T. E. Beechem, "Effects of surface roughness and oxide layer on the thermal boundary conductance at aluminum/silicon interfaces," *Phys. Rev. B* **82**, 085307 (2010).
- ¹⁶ P. E. Hopkins, J. C. Duda, C. W. Petz, and J. A. Floro, "Controlling thermal conductance through quantum dot roughening at interfaces," *Phys. Rev. B* **84**, 035438 (2011).

- ¹⁷ J. C. Duda and P. E. Hopkins, "Systematically controlling Kapitza conductance via chemical etching," *Appl. Phys. Lett.* **100**, 111602 (2012).
- ¹⁸ M. D. Losego, M. E. Grady, N. R. Sottos, D. G. Cahill, and P. V. Braun, "Effects of chemical bonding on heat transport across interfaces," *Nat. Mater.* **11**, 502–506 (2012).
- ¹⁹ P. E. Hopkins, M. Baraket, E. V. Barnat, T. E. Beechem, S. P. Kearney, J. C. Duda, J. T. Robinson, and S. G. Walton, "Manipulating thermal conductance at metal-graphene contacts via chemical functionalization," *Nano Lett.* **12**, 590–595 (2012).
- ²⁰ B. M. Foley, S. C. Hernández, J. C. Duda, J. T. Robinson, S. G. Walton, and P. E. Hopkins, "Modifying surface energy of graphene via plasma-based chemical functionalization to tune thermal and electrical transport at metal interfaces," *Nano Lett.* **15**, 4876–4882 (2015).
- ²¹ J. C. Duda, C.-Y. P. Yang, B. M. Foley, R. Cheaito, D. L. Medlin, R. E. Jones, and P. E. Hopkins, "Influence of interfacial properties on thermal transport at gold:silicon contacts," *Appl. Phys. Lett.* **102**, 081902 (2013).
- ²² J. A. Tomko, A. Giri, B. F. Donovan, D. M. Bubb, S. M. O'Malley, and P. E. Hopkins, "Energy confinement and thermal boundary conductance effects on short-pulsed thermal ablation thresholds in thin films," *Phys. Rev. B* **96**, 014108 (2017).
- ²³ P. J. O'Brien, S. Shenogin, J. Liu, P. K. Chow, D. Laurencin, P. H. Mutin, M. Yamaguchi, P. Koblinski, and G. Ramanath, "Bonding-induced thermal conductance enhancement at inorganic heterointerfaces using nanomolecular monolayers," *Nat. Mater.* **12**, 118–122 (2013).
- ²⁴ J. C. Duda, T. S. English, E. S. Piekos, W. A. Soffa, L. V. Zhigilei, and P. E. Hopkins, "Implications of cross-species interactions on the temperature dependence of Kapitza conductance," *Phys. Rev. B* **84**, 193301 (2011).
- ²⁵ A. Giri, J. L. Braun, and P. E. Hopkins, "Implications of interfacial bond strength on the spectral contributions to thermal boundary conductance across solid, liquid, and gas interfaces: A molecular dynamics study," *J. Phys. Chem. C* **120**, 24847–24856 (2016).
- ²⁶ S. G. Walton, B. M. Foley, S. Hernandez, D. Boris, M. Baraket, J. C. Duda, J. T. Robinson, and P. E. Hopkins, "Plasma-based chemical functionalization of graphene to control the thermal transport at graphene-metal interfaces," *Surf. Coat. Technol.* **314**, 148–154 (2017).
- ²⁷ C. S. Gorham, K. Hattar, R. Cheaito, J. C. Duda, J. T. Gaskins, T. E. Beechem, J. F. Ihlefeld, L. B. Biedermann, E. S. Piekos, D. L. Medlin, and P. E. Hopkins, "Ion irradiation of the native oxide/silicon surface increases the thermal boundary conductance across aluminum/silicon interfaces," *Phys. Rev. B* **90**, 024301 (2014).
- ²⁸ P. E. Hopkins, J. C. Duda, S. P. Clark, C. P. Hains, T. J. Rotter, L. M. Phinney, and G. Balakrishnan, "Effect of dislocation density on thermal boundary conductance across GaSb/GaAs interfaces," *Appl. Phys. Lett.* **98**, 161913 (2011).
- ²⁹ J. T. Gaskins, A. Bulusu, A. J. Giordano, J. C. Duda, S. Graham, and P. E. Hopkins, "Thermal conductance across phosphonic acid molecules and interfaces: Ballistic versus diffusive vibrational transport in molecular monolayers," *J. Phys. Chem. C* **119**, 20931–20939 (2015).
- ³⁰ J. C. Duda, T. S. English, E. S. Piekos, T. E. Beechem, T. W. Kenny, and P. E. Hopkins, "Bidirectionally tuning Kapitza conductance through the inclusion of substitutional impurities," *J. Appl. Phys.* **112**, 073519 (2012).
- ³¹ T. E. Beechem, S. Graham, P. E. Hopkins, and P. M. Norris, "The role of interface disorder on thermal boundary conductance using a virtual crystal approach," *Appl. Phys. Lett.* **90**, 054104 (2007).
- ³² P. E. Hopkins, P. M. Norris, R. J. Stevens, T. Beechem, and S. Graham, "Influence of interfacial mixing on thermal boundary conductance across a chromium/silicon interface," *J. Heat Transfer* **130**, 062402 (2008).
- ³³ C. J. Szejewski, N. C. Creange, K. Sun, A. Giri, B. F. Donovan, C. Constantin, and P. E. Hopkins, "Size effects in the thermal conductivity of gallium oxide (β -Ga₂O₃) films grown via open-atmosphere annealing of gallium nitride," *J. Appl. Phys.* **117**, 084308 (2015).
- ³⁴ B. L. French and S. W. King, "Detection of surface electronic defect states in low and high-k dielectrics using reflection electron energy loss spectroscopy," *J. Mater. Res.* **28**, 2271–2784 (2013).
- ³⁵ J. H. Yum, T. Akyol, M. Lei, D. A. Ferrer, T. W. Hudnall, M. Downer, C. W. Bielawski, G. Bersuker, J. C. Lee, and S. K. Banerjee, "A study of highly crystalline novel beryllium oxide film using atomic layer deposition," *J. Cryst. Growth* **334**, 126–133 (2011).
- ³⁶ J. H. Yum, T. Akyol, M. Lei, D. A. Ferrer, T. W. Hudnall, M. Downer, C. W. Bielawski, G. Bersuker, J. C. Lee, and S. K. Banerjee, "Electrical and physical characteristics for crystalline atomic layer deposited beryllium oxide thin film on Si and GaAs substrates," *Thin Solid Films* **520**, 3091–3095 (2012).
- ³⁷ J. L. van Hemmen, S. B. S. Heil, J. H. Klootwijk, F. Roozeboom, C. J. Hodson, M. C. M. van de Sanden, and W. M. M. Kessels, "Plasma and thermal ALD of Al₂O₃ in a commercial 200 mm ALD reactor," *J. Electrochem. Soc.* **154**, G165–G169 (2007).
- ³⁸ D. G. Cahill, "Analysis of heat flow in layered structures for time-domain thermoreflectance," *Rev. Sci. Instrum.* **75**, 5119–5122 (2004).
- ³⁹ K. Kang, Y. K. Koh, C. Chirutescu, X. Zheng, and D. G. Cahill, "Two-tint pump-probe measurements using a femtosecond laser oscillator and sharp-edged optical filters," *Rev. Sci. Instrum.* **79**, 114901 (2008).
- ⁴⁰ P. E. Hopkins, J. R. Serrano, L. M. Phinney, S. P. Kearney, T. W. Grasser, and C. T. Harris, "Criteria for cross-plane dominated thermal transport in multilayer thin film systems during modulated laser heating," *J. Heat Transfer* **132**, 081302 (2010).
- ⁴¹ A. J. Schmidt, "Pump-probe thermoreflectance," *Annu. Rev. Heat Transfer* **16**, 159–181 (2013).
- ⁴² W. A. Lanford, M. Parenti, B. J. Nordell, M. M. Paquette, A. N. Caruso, M. Mäntymäki, J. Hämäläinen, M. Ritala, K. B. Klepper, V. Miikkulainen, O. Nilsen, W. Tenhaeff, N. Dudney, D. Koh, S. K. Banerjee, E. Mays, J. Bielefeld, and S. W. King, "Nuclear reaction analysis for H, Li, Be, B, C, N, O and F with an RBS check," *Nucl. Instrum. Methods Phys. Res., Sect. B* **371**, 211–215 (2016).
- ⁴³ S. W. King, J. Bielefeld, M. French, and W. A. Lanford, "Mass and bond density measurements for PECVD a-SiC_x:H thin films using Fourier transform-infrared spectroscopy," *J. Non-Cryst. Solids* **357**, 3602–3615 (2011).

- ⁴⁴ K. An, K. S. Ravichandran, R. E. Dutton, and S. L. Semiatin, "Microstructure, texture, and thermal conductivity of single-layer and multilayer thermal barrier coatings of Y_2O_3 -stabilized ZrO_2 and Al_2O_3 made by physical vapor deposition," *J. Am. Ceram. Soc.* **82**, 399–406 (1999).
- ⁴⁵ C. Thomsen, J. Strait, Z. Vardeny, H. J. Maris, J. Tauc, and J. J. Hauser, "Coherent phonon generation and detection by picosecond light pulses," *Phys. Rev. Lett.* **53**, 989–992 (1984).
- ⁴⁶ C. Thomsen, H. J. Maris, and J. Tauc, "Picosecond acoustics as a non-destructive tool for the characterization of very thin films," *Thin Solid Films* **154**, 217–223 (1987).
- ⁴⁷ S.-M. Lee and D. G. Cahill, "Heat transport in thin dielectric films," *J. Appl. Phys.* **81**, 2590–2595 (1997).
- ⁴⁸ D. R. G. Mitchell, G. Triani, D. J. Attard, K. S. Finnie, P. J. Evans, C. J. Barbé, and J. R. Bartlett, "Atomic layer deposition of TiO_2 and Al_2O_3 thin films and nanolaminates," *Smart Mater. Struct.* **15**, S57 (2006).
- ⁴⁹ R. Cheaito, J. T. Gaskins, M. E. Caplan, B. F. Donovan, B. M. Foley, A. Giri, J. C. Duda, C. J. Szejewski, C. Constantin, H. J. Brown-Shaklee, J. F. Ihlefeld, and P. E. Hopkins, "Thermal boundary conductance accumulation and interfacial phonon transmission: Measurements and theory," *Phys. Rev. B* **91**, 035432 (2015).
- ⁵⁰ G. Chen, "Thermal conductivity and ballistic-phonon transport in the cross-plane direction of superlattices," *Phys. Rev. B* **57**, 14958–14973 (1998).
- ⁵¹ J. C. Duda, T. Beechem, J. L. Smoyer, P. M. Norris, and P. E. Hopkins, "The role of dispersion on phononic thermal boundary conductance," *J. Appl. Phys.* **108**, 073515 (2010).
- ⁵² J. C. Duda, P. E. Hopkins, J. L. Smoyer, M. L. Bauer, T. S. English, C. B. Saltonstall, and P. M. Norris, "On the assumption of detailed balance in prediction of diffusive transmission probability during interfacial transport," *Nanoscale Microscale Thermophys. Eng.* **14**, 21–33 (2010).
- ⁵³ S.-M. Lee, D. G. Cahill, and T. H. Allen, "Thermal conductivity of sputtered oxide films," *Phys. Rev. B* **52**, 253–257 (1995).
- ⁵⁴ M. W. J. Chase, *NIST-JANAF Thermochemical Tables*, 4th ed., Journal of Physical and Chemical Reference Data Monographs or Supplements (1998), Vol. 9, pp. 1–1951.
- ⁵⁵ C. Wang, M. Zinkevich, and F. Aldinger, "The zirconia-hafnia system: DTA measurements and thermodynamic calculations," *J. Am. Ceram. Soc.* **89**, 3751–3758 (2006).
- ⁵⁶ P. Flubacher, A. J. Leadbetter, and J. A. Morrison, "The heat capacity of pure silicon and germanium and properties of their vibrational frequency spectra," *Philos. Mag.* **4**, 273–294 (1959).
- ⁵⁷ N. H. Nickel, *Laser Crystallization of Silicon—Fundamentals to Devices* (Academic Press, New York, 2003).